INL/JOU-18-45118-Revision-1

Predicting Calendar Aging in Lithium Metal Secondary Batteries: The Impacts of Solid Electrolyte Interphase Composition and Stability

Eric J. Dufek, Shrikant C. Nagpure, Sergiy V. Sazhin, Boryann Liaw, Y. Shirley Meng, Sean M. Wood, Chengcheng Fang

August 2018

The INL is a U.S. Department of Energy National Laboratory
operated by Battelle Energy Alliance

Idaho National Laboratory

INL/JOU-18-45118-Revision-1

Predicting Calendar Aging in Lithium Metal Secondary Batteries: The Impacts of Solid Electrolyte Interphase Composition and Stability

Eric J. Dufek, Shrikant C. Nagpure, Sergiy V. Sazhin, Boryann Liaw, Y. Shirley Meng, Sean M. Wood, Chengcheng Fang

August 2018

Idaho National Laboratory
Idaho Falls, Idaho 83415

http://www.inl.gov

Prepared for the
U.S. Department of Energy
Office of Energy Efficiency and Renewable Energy
Under DOE Idaho Operations Office
Contract DE-AC07-05ID14517

ADVANCED ENERGY MATERIALS
www.advenergymat.de

Predicting Calendar Aging in Lithium Metal Secondary Batteries: The Impacts of Solid Electrolyte Interphase Composition and Stability

Sean M. Wood, Chengcheng Fang, Eric J. Dufek, Shrikant C. Nagpure, Sergiy V. Sazhin, Boryann Liaw, and Y. Shirley Meng*

Calendar aging of lithium metal batteries, in which cells' components degrade internally due to chemical reactions while no current is being applied, is a relatively unstudied field. In this work, a model to predict calendar aging of lithium metal cells is developed using two sets of readily obtainable data: solid electrolyte interphase (SEI) layer composition (measured via X-ray photoelectron spectroscopy) and SEI stability (measured as a degradation rate using a simple constant current–constant voltage charging protocol). Electrolyte properties such as volume and salt concentration are varied in order to determine their effect on SEI stability and composition, with subsequent impacts to calendar aging. Lower salt concentrations produce a solvent-based, more soluble SEI, while the highest concentration produces a salt-based, less soluble SEI. Higher electrolyte volumes promote dissolution of the SEI and thus decrease its stability. The model predicts that lithium metal would be the limiting factor in calendar aging, depleting long before the electrolyte does. Additionally, the relative composition of the electrolyte during aging is modeled and found to eventually converge to the same value independent of initial salt concentration.

Rechargeable Li-ion batteries are ubiquitous throughout modern society, and there is continuing consumer demand to increase their specific energy to significantly higher values. Recently, the US Department of Energy created a program that has a stated goal of developing rechargeable lithium battery technology that can achieve a specific energy of 500 Wh kg^{-1}.[1] Lithium metal is a prime candidate for advancing toward this goal due to its superior characteristics over the state-of-the-art graphite: 10× higher capacity than graphite, more negative redox potential, and lighter weight.[2–6]

Dr. S. M. Wood, Dr. E. J. Dufek, Dr. S. C. Nagpure, Dr. S. V. Sazhin, Dr. B. Liaw
Energy Storage and Advanced Vehicles Department
Idaho National Laboratory
Idaho Falls, ID 83415, USA
E-mail: eric.dufek@inl.gov
C. Fang, Prof. Y. S. Meng
Department of NanoEngineering
University of California San Diego
La Jolla, CA 92093, USA
The ORCID identification number(s) for the author(s) of this article can be found under https://doi.org/10.1002/aenm.201801427.

DOI: 10.1002/aenm.201801427

Despite its advantages, lithium metal is a particularly challenging anode material due to its high reactivity.[2,5–9] Nearly all known electrolyte solvents and salts reduce on the surface of lithium to form a solid electrolyte interphase (SEI) layer.[5,10] During cycling, lithium continually consumes electrolyte to generate SEI; as such, reduced electrolyte volumes have been shown to result in premature cell failure as the electrolyte dries out.[2,6,7,11,12] One route investigated to minimize this consumption has been the use of ether-based electrolytes with high salt concentrations that have shown improved Coulombic efficiency.[2,3,13–15] However, the limited initial supplies of lithium metal and electrolyte combined with their high reactivity may result in significant depletion of these resources long before cycling ever takes place. Although many researchers have examined how electrolyte volume and salt concentration affect cycle life and lithium deposit morphology, none have examined its role on calendar aging, which is the degradation of a battery during the rest state when no current is being applied.[16] During calendar aging, chemical rather than electrochemical reactions are responsible for the degradation of the cell components, in this case the consumption of lithium metal and electrolyte as they react with each other to generate and regenerate an ever-evolving SEI layer. Depending on the severity of this consumption, calendar aging can have a large negative impact on the electrochemical cycling of the cell.

In order to develop a model to predict calendar aging in lithium metal cells, two sets of information were needed: the dependence of SEI composition on electrolyte salt concentration (since the electrolyte concentration changes during aging) and the time dependence of the SEI degradation rate. In the first part of this work, $dQ\,dV^{-1}$ profiles and X-ray photoelectron spectroscopy (XPS) data were used to examine the role that salt concentration plays in SEI composition. Similarly to the work of Nie et al.,[17] the salt concentration was found to drive the overall composition of the SEI toward one of two regimes, one solvent-based and one salt-based. In the second part of this work, a simple constant current–constant voltage (CC–CV) charging protocol was used to measure the degradation rate of the SEI, finding that lower electrolyte volumes and a salt-based SEI produced the

 © 2018 WILEY-VCH Verlag GmbH & Co. KGaA, Weinheim

most stable SEI layer. In the last part of this work, these two sets of information were combined to develop the model and make predictions about lithium metal battery calendar aging based on charge consumed to generate SEI by reaction with lithium metal and electrolyte, separately, as well as how the electrolyte composition changes during said aging. Lithium metal was predicted to be the limiting factor in calendar aging, depleting an order of magnitude faster than the electrolyte. Additionally, the electrolyte always converged to the same composition at the end of aging, no matter the original salt concentration. The authors believe this work is the first to make predictions about lithium secondary battery calendar aging using readily measured SEI composition and degradation properties.

The first set of information needed for the calendar aging model was collected: salt concentration-dependent SEI composition information derived from $dQ\ dV^{-1}$ and XPS data. The electrolyte used in this work was a 3:7 (w/w) mixture of ethylene carbonate (EC) and ethyl methyl carbonate (EMC) with 2 wt% of vinylene carbonate (VC) into which varying concentrations of $LiPF_6$ were dissolved (0.5, 1.2, and 3.6 M). Typically, Li ‖ Cu cells are used for SEI and lithium plating studies on the Cu substrate, but lithium's highly reactive and inherently variable surface can lead to measurement inconsistencies in this cell configuration. In this work, $LiFePO_4$ was used as the source for lithium to mitigate the aforementioned variability.[8,18] **Figure 1**a shows, as a comparative example, the differential capacity profiles for SEI formation on the surface of Cu foil in Li ‖ Cu and Cu ‖ $LiFePO_4$ cells. In Li ‖ Cu cells, the voltage progresses from open circuit (≈3.0 V; the circle on the plot) down to 0.0 V, exhibiting four sequential peaks. In the Cu ‖ $LiFePO_4$ cell, this voltage trace is rotated by 180°; the voltage increases from open circuit (≈0.4 V) up to the cutoff of 3.4 V, exhibiting the same four sequential peaks.

The differential capacity profiles for the three salt concentrations in the Cu ‖ $LiFePO_4$ cells are shown in Figure 1b for an electrolyte volume of 16 µL (data for all volumes and concentrations can be found in Figure S3 in the Supporting Information). The bottom axis in Figure 1b is the actual measured voltage of the cell, whereas the top axis is the equivalent potential in a Li ‖ Cu cell. The peaks above 1.8 V in the plots (corresponding to less than roughly 1.6 V in a Li ‖ Cu cell) are in a solvent-based SEI regime and relate to the reduction of EC and VC,[19,20] whereas the peaks at voltages below 1.8 V are in a salt-based reduction regime and relate to the reduction of $LiPF_6$.[17] Some examples (a nonexhaustive list) of chemical and electrochemical SEI formation reactions are shown below; Equation (1)–(3) are in the solvent-based regime while Equations (4) and (5) are in the salt-based regime.[21–28] The peaks in Figure 1b demonstrate that the majority of the charge consumed for SEI growth at the two lower salt concentrations went toward forming solvent-based SEI components while at the highest concentration mostly salt-based components were formed.

$$n\mathrm{EC} + 2\mathrm{Li}^+ + 2\mathrm{e}^- \rightarrow \mathrm{LiO}(-\mathrm{CH_2}-\mathrm{CH_2}-\mathrm{O}-)_n\,\mathrm{Li}\downarrow + n\mathrm{CO_2}\uparrow \quad (1)$$

$$2\mathrm{EC} + 2\mathrm{Li}^+ + 2\mathrm{e}^- \rightarrow (\mathrm{CH_2OCO_2Li})_2\downarrow + \mathrm{C_2H_4}\uparrow \quad (2)$$

$$1\mathrm{EC} + 2\mathrm{Li}^+ + 2\mathrm{e}^- \rightarrow \mathrm{Li_2CO_3}\downarrow + \mathrm{C_2H_4}\uparrow \quad (3)$$

$$\mathrm{LiPF_6} \rightarrow \mathrm{LiF}\downarrow + \mathrm{PF_5}\uparrow \quad (4)$$

$$\mathrm{PF_5} + n\mathrm{Li}^+ + n\mathrm{e}^- \rightarrow \mathrm{LiF}\downarrow + \mathrm{Li}_x\mathrm{PF}_y\downarrow \quad (5)$$

The preference for one SEI regime over another is caused by differences in the solvation of Li-ions within the electrolyte solution. At a concentration of 0.5 M, there are more than seven EC molecules available per Li-ion. Therefore, Li-ions will be solvated in the well-known tetrahedral configuration[29,30] by four EC molecules, forming a solvent-separated ion pair in which the PF_6^- anion is separated from the Li^+ cation by the sheath of molecules solvating it: $Li(EC)_4^+$.[15,17,30] At 1.2 M, the number of available EC molecules per Li-ion decreases to only three. With fewer than four EC molecules able to solvate it, an EMC molecule takes the place of one of the EC molecules in the tetrahedral solvation shell, forming another solvent-separated ion pair: $Li(EC)_3(EMC)^+$.[15,30] At the highest concentration of 3.6 M, there is only one EC molecule available per Li-ion, leading the PF_6^- anion to enter the solvation shell to form a contact ion pair: $Li(EC)(EMC)_2PF_6$.[15,17,30] At the two lower concentrations, the high number of EC molecules and absence of PF_6^- in the solvation shell lead to a preference for the reduction of EC at the anode surface, precipitating solvent-based products. At the highest concentration, the presence of PF_6^- in the solvation sheath leads to its participation in SEI formation, generating salt-based SEI.[15,17]

XPS is a commonly used technique to examine the outermost surface (≈10 nm) of the SEI layer,[31] and it was used here to chemically confirm the existence of the two SEI regimes. XPS was performed following the SEI maturation protocol (described in the Supporting Information) and repeated lithium plating/stripping, and the C 1s and F 1s spectra are shown in Figure 1c,d, respectively. The remaining spectra (O 1s, Li 1s, and P 2p) are shown in Figure S4 in the Supporting Information along with a table of all peak assignments and relevant references in Table S3 in the Supporting Information. The C 1s spectra showed the SEI was comprised of five carbon-containing components: adventitious carbon (C—C/C—H), poly(ethylene oxide) (PEO), Li_2CO_3, $(CH_2OCO_2Li)_2$, and poly(vinylene carbonate) (poly(VC)). PEO, Li_2CO_3, and $(CH_2OCO_2Li)_2$ are reduction products of EC[21] while poly(VC) is a reduction product of VC.[22] The F 1s spectra showed the SEI contained three $LiPF_6$-derived reduction products: LiF, $Li_xPO_yF_z$, and Li_xPF_y.[23,24] The area under the C 1s spectra decreased by about 28% upon increasing the concentration to 3.6 M, while the area under the F 1s spectra increased by 501%. Because the C 1s and F 1s spectra are comprised solely of either EC/VC-based or $LiPF_6$-based reduction products, respectively, their areal ratio ($A_{C\ 1s}$ / $A_{F\ 1s}$, denoted as C/F) can serve as a proxy for the relative amounts of solvent-based and salt-based SEI, where a higher C/F ratio signifies a more solvent-based SEI. XPS areal ratios have been used to characterize cathodes in the past,[32–34] but their use to compare two distinct types of SEI (via the C/F ratio) is novel. The C/F ratio was 3.8 at 0.5 M, 3.5 at 1.2 M, and 0.4 at 3.6 M, indicating the SEI was primarily solvent-based at the lower concentrations but became predominantly salt-based at the highest concentration.

© 2018 WILEY-VCH Verlag GmbH & Co. KGaA, Weinheim

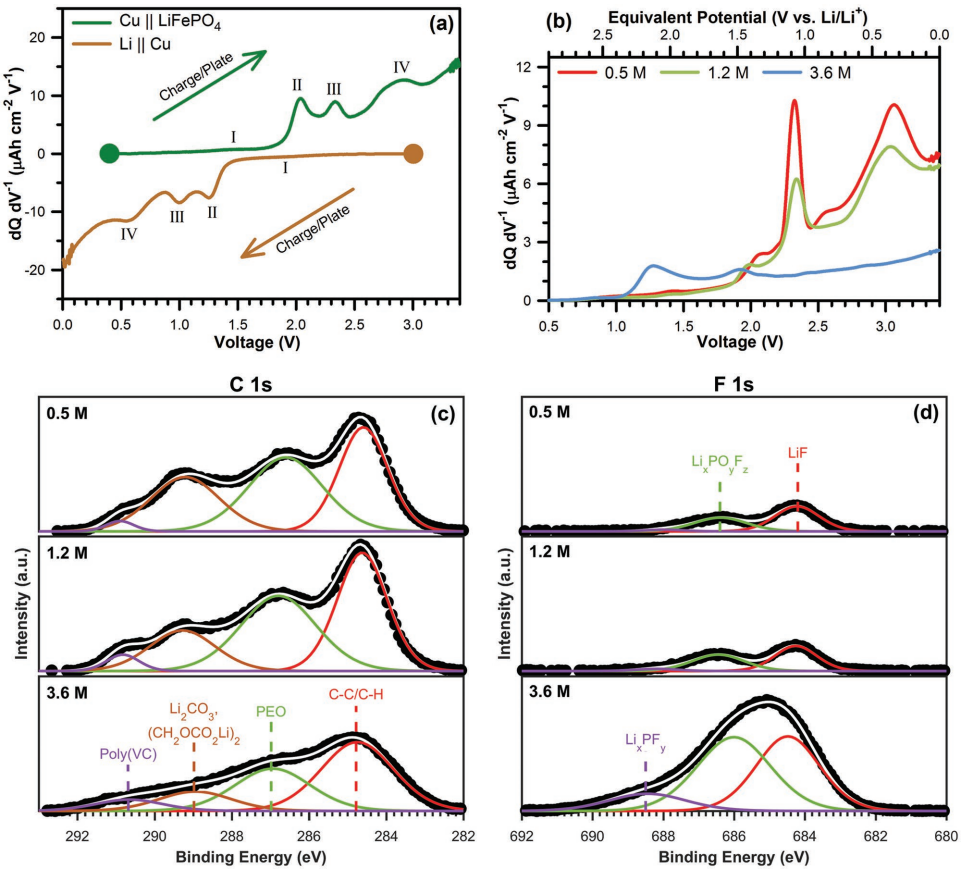

Figure 1. a) Differential capacity profiles of SEI formation in Li || Cu cells and Cu || $LiFePO_4$ cells. Dots indicate open circuit voltage. b) Differential capacity profiles of the first SEI formation cycle in Cu || $LiFePO_4$ cells with 16 µL of electrolyte with varying $LiPF_6$ concentrations. For other volumes, please see the Supporting Information. c) C 1s and d) F 1s XPS spectra of the SEI on copper foil after plating/stripping lithium several times.

In order to gather the second set of data required for the calendar aging model, a repeated CC–CV charging protocol (see the Supporting Information) was used to measure SEI degradation properties, and the results are shown in **Figure 2** and Figure S5 in the Supporting Information.[35] During each CC–CV repetition, charge was consumed to grow SEI on the copper substrate; the cycle-by-cycle and cumulative capacities dedicated to SEI formation are shown in Figure S5a,b in the Supporting Information, respectively. In the succeeding rest step of each CC–CV repetition, portions of the SEI dissolved into the electrolyte or were otherwise degraded. These portions must then be repaired or maintained. The SEI degradation rate was calculated by dividing the charge required to repair the SEI (i.e., the amount that was assumed to have degraded) by the time of the rest period over which the degradation occurred. The cycle-by-cycle and pseudo-steady-state (found at the 26th cycle) degradation rates are shown in Figure 2a,b, respectively.

Both the formation capacity and degradation rate exhibited a power-law decay throughout the CC–CV repetitions, indicating that the soluble SEI components were being replaced

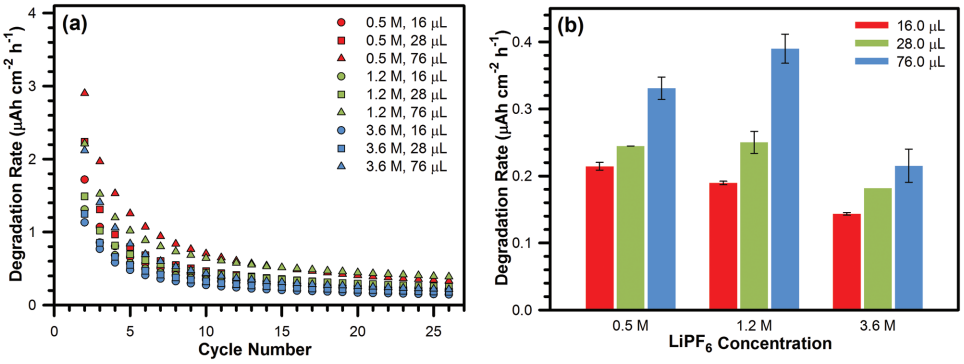

Figure 2. a) Cycle-by-cycle SEI degradation rate. b) 26th cycle SEI degradation rate.

© 2018 WILEY-VCH Verlag GmbH & Co. KGaA, Weinheim

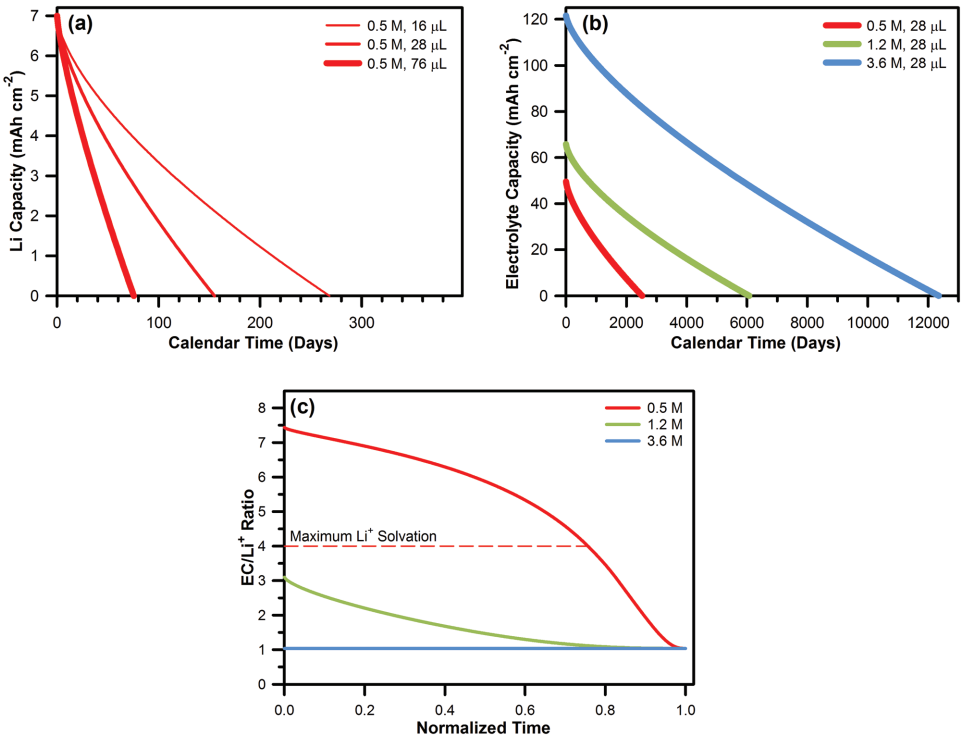

Figure 3. a) Predicted calendar aging of lithium metal cells based on Li metal consumption with an initial Li capacity of 7 mAh cm^{-2} for the 0.5 M concentration, using the model developed from XPS and degradation rate data. Curves for 1.2 and 3.6 M concentrations can be found in Figure S6a, b in the Supporting Information, respectively. b) Predicted calendar aging of lithium metal cells based on electrolyte consumption for the 28 µL volume. Curves for the 16 µL volume can be found in Figure S6c in the Supporting Information. Initial capacities of the electrolyte were calculated from the given volumes and salt concentrations. c) Predicted changes in the EC/Li^+ ratio within the electrolyte versus normalized time.

by insoluble compounds, leading to an increasingly stable SEI. Electrolyte volume and salt concentration are both possible factors affecting the stability of the various SEI components against dissolution. Typically, higher liquid volumes promote dissolution of solid compounds by shifting the solubility equilibria while higher salt concentrations tend to suppress dissolution. With regards to SEI degradation rate (Figure 2b), the former held true; the dissolution of SEI components increased with increasing volume of electrolyte. However, the degradation rate did not exhibit the expected decrease when the salt concentration increased from 0.5 to 1.2 M. The degradation rate decreased substantially at 3.6 M, but this effect was most likely due to the comparatively insoluble salt-based SEI rather than the dissolution suppressing effects of a higher salt concentration. Total SEI formation capacity (Figure S5b, Supporting Information) exhibited similar trends as the degradation rate; higher degradation rates meant that more charge was consumed to form a stabilized SEI.

These composition and stability factors have cell design implications; for example, shelf life can be reduced if an unstable SEI is continually consuming Li and electrolyte to regenerate itself. To this end, an extrapolation of the power-law fitting of the SEI formation capacity data, combined with the C/F ratio data derived from XPS, was used to develop a model to predict calendar aging of lithium cells as shown in **Figure 3**. To understand calendar aging, two boundary conditions exist; one in which charge to form the SEI is entirely consumed by reaction of the lithium metal anode and one where charge to form the SEI is solely consumed by the reaction of the electrolyte. Separating the consumption of lithium metal and electrolyte allows for identification of one or the other as the limiting factor in calendar aging; in reality, these reactions would occur concurrently.

In Figure 3a, calendar life was predicted for the 0.5 M electrolyte by assuming that all of the SEI formation charge was consumed exclusively by reaction of 7 mAh cm^{-2} of lithium metal (100% excess of a theoretical high capacity cathode of 3.5 mAh cm^{-2}), ignoring charge consumption by electrolyte. Predictions for the 1.2 and 3.6 M electrolytes can be found in Figure S6a,b, respectively. Calendar life for this theoretical anode ranged from 80 to 380 d before the lithium metal was completely consumed. At the lowest salt concentration calendar life decreased with increasing volume, as expected due to the similar trend in degradation rate; a more stable SEI translates to a longer calendar life. This trend was not observed at the two higher concentrations. Because of the different power-law fittings of the degradation curves (e.g., the degradation rates were similar for 1.2 M, 76 µL and 3.6 M, 76 µL at cycle 1 but very different at cycle 26), the extrapolated aging curves did not necessarily follow the same trend as the snapshot at the 26th cycle.

Calendar life of a lithium metal cell based solely on consumption of electrolyte to generate SEI (ignoring lithium metal consumption) can also be calculated by converting the volume of electrolyte and its concentration into a capacity using some assumptions about the SEI formation reactions (see the Supporting Information). These curves are shown in Figure 3b for the 28 µL volume; data for 16 µL can be found in Figure S6c

© 2018 WILEY-VCH Verlag GmbH & Co. KGaA, Weinheim

in the Supporting Information. In this case, calendar life based on electrolyte consumption was strongly correlated to its initial capacity; higher volumes and higher salt concentrations had higher capacities and thus longer calendar life. These calendar lifetimes lasted from 2200 to more than 12 000 d, indicating that formation of SEI by consumption of lithium metal will likely be the limiting factor in the shelf life of a lithium metal battery, rather than consumption of electrolyte.

In Figure S6d in the Supporting Information, the 16 µL data from Figure S6c in the Supporting Information was split into solvent- and salt-based components in order to track their depletion individually. One might expect that an electrolyte in the solvent-based SEI regime would preferentially consume the electrolyte solvents until they are depleted, and vice versa for the salt-based SEI regime, but this was not the case. The concentrations of the individual components converged throughout aging, eventually depleting simultaneously. As either solvent- or salt-based electrolyte components were preferentially consumed, the relative EC/Li^+ ratio in the electrolyte changed and could be modeled as well; this ratio is shown versus normalized time in Figure 3c. The lower the initial concentration of $LiPF_6$, the more rapidly the EC/Li^+ ratio changed. At the highest concentration, the ratio was relatively constant throughout aging. Interestingly, the ratio converged to the same value at the end of aging for all concentrations.

In this work, data on the effects of electrolyte volume and salt concentration on SEI composition and stability were collected and used to develop a model to predict calendar aging in lithium metal batteries. The SEI composition experienced a marked shift from solvent- to salt-based reduction products upon increasing the salt concentration. In general, larger volumes of electrolyte shifted the solubility equilibria of the SEI components, leading to higher dissolution and lowered SEI stability. The salt-based SEI produced by the highest concentration electrolyte was more stable against dissolution. When these data were used to develop the model, it was found that lithium metal would be the limiting factor in calendar aging. Additionally, the electrolyte composition was not fixed and always converged to the same EC/Li^+ ratio, no matter the initial salt concentration. The results of this model likely represent a best-case scenario for calendar lifetimes; once cycling begins, large increases in surface area will lead to more rapid consumption of the lithium metal anode and electrolyte, resulting in accelerated calendar aging. To date, little attention has been paid to calendar aging in lithium metal batteries. This work shows that, due to the extreme reactivity of lithium, the electrolyte plays a key role in the calendar aging process and should become a focus going forward for researchers looking to develop novel electrolytes.

Supporting Information

Supporting Information is available from the Wiley Online Library or from the author.

Acknowledgements

Research was supported by the Assistant Secretary for Energy Efficiency and Renewable Energy, Office of Vehicle Technologies of the U.S. Department of Energy through the Advanced Battery Materials Research (BMR) Program (Battery500 Consortium). INL is operated by Battelle Energy Alliance under Contract Nos. DE-DE-AC07-05ID14517 for the U.S. Department of Energy. XPS was performed at University of California, Irvine Materials Research Institute (IMRI) using instrumentation funded in part by the National Science Foundation Major Research Instrumentation Program under grant no. CHE-1338173. The UCSD team would like to thank Dr. Ich Tran for his assistance in performing XPS measurement.

Conflict of Interest

The authors declare no conflict of interest.

Keywords

electrolyte volume, electrolyte salt concentration, lithium metal calendar life, rechargeable lithium batteries, solid electrolyte interphase (SEI) layer stability

Received: May 11, 2018
Revised: July 7, 2018
Published online:

[1] U. S. DRIVE, Electrochemical Energy Storage Technical Team Roadmap (September 2017), https://www.energy.gov/eere/vehicles/us-drive-partnership-plan-roadmaps-and-accomplishments (accessed: January 2018).
[2] S. S. Zhang, *ACS Appl. Energy Mater.* **2018**, *1*, 910.
[3] J. Qian, W. A. Henderson, W. Xu, P. Bhattacharya, M. Engelhard, O. Borodin, J.-G. Zhang, *Nat. Commun.* **2015**, *6*, 6362.
[4] P. Albertus, S. Babinec, S. Litzelman, A. Newman, *Nat. Energy* **2017**, *3*, 16.
[5] A. Pei, G. Zheng, F. Shi, Y. Li, Y. Cui, *Nano Lett.* **2017**, *17*, 1132.
[6] K.-H. Chen, K. N. Wood, E. Kazyak, W. S. LePage, A. L. Davis, A. J. Sanchez, N. P. Dasgupta, *J. Mater. Chem. A* **2017**, *5*, 11671.
[7] J. Zheng, P. Yan, D. Mei, M. H. Engelhard, S. S. Cartmell, B. J. Polzin, C. Wang, J.-G. Zhang, W. Xu, *Adv. Energy Mater.* **2016**, *6*, 1502151.
[8] J. Qian, B. D. Adams, J. Zheng, W. Xu, W. A. Henderson, J. Wang, M. E. Bowden, S. Xu, J. Hu, J.-G. Zhang, *Adv. Funct. Mater.* **2016**, *26*, 7094.
[9] K. N. Wood, E. Kazyak, A. F. Chadwick, K.-H. Chen, J.-G. Zhang, K. Thornton, N. P. Dasgupta, *ACS Cent. Sci.* **2016**, *2*, 790.
[10] B. D. Adams, J. Zheng, X. Ren, W. Xu, J.-G. Zhang, *Adv. Energy Mater.* **2018**, *8*, 1702097.
[11] H. Pan, K. S. Han, M. H. Engelhard, R. Cao, J. Chen, J.-G. Zhang, K. T. Mueller, Y. Shao, J. Liu, *Adv. Funct. Mater.* **2018**, 1707234, https://doi.org/10.1002/adfm.201707234.
[12] D. Lu, Y. Shao, T. Lozano, W. D. Bennett, G. L. Graff, B. Polzin, J. Zhang, M. H. Engelhard, N. T. Saenz, W. A. Henderson, P. Bhattacharya, J. Liu, J. Xiao, *Adv. Energy Mater.* **2015**, *5*, 1400993.
[13] L. Suo, Y.-S. Hu, H. Li, M. Armand, L. Chen, *Nat. Commun.* **2013**, *4*, 1481.
[14] J. Wang, Y. Yamada, K. Sodeyama, C. H. Chiang, Y. Tateyama, A. Yamada, *Nat. Commun.* **2016**, *7*, 12032.
[15] J. Zheng, J. A. Lochala, A. Kwok, Z. D. Deng, J. Xiao, *Adv. Sci.* **2017**, *4*, 1700032.
[16] P. Keil, S. F. Schuster, J. Wilhelm, J. Travi, A. Hauser, R. C. Karl, A. Jossen, *J. Electrochem. Soc.* **2016**, *163*, A1872.
[17] M. Nie, D. P. Abraham, D. M. Seo, Y. Chen, A. Bose, B. L. Lucht, *J. Phys. Chem. C* **2013**, *117*, 25381.
[18] Z. L. Brown, S. Jurng, B. L. Lucht, *J. Electrochem. Soc.* **2017**, *164*, A2186.

© 2018 WILEY-VCH Verlag GmbH & Co. KGaA, Weinheim

[19] M. Nie, J. Demeaux, B. T. Young, D. R. Heskett, Y. Chen, A. Bose, J. C. Woicik, B. L. Lucht, *J. Electrochem. Soc.* **2015**, *162*, A7008.
[20] X. Zhang, R. Kostecki, T. J. Richardson, J. K. Pugh, P. N. Ross, *J. Electrochem. Soc.* **2001**, *148*, A1341.
[21] S. M. Wood, C. H. Pham, R. Rodriguez, S. S. Nathan, A. D. Dolocan, H. Celio, J. P. de Souza, K. C. Klavetter, A. Heller, C. B. Mullins, *ACS Energy Lett.* **2016**, *1*, 414.
[22] L. El Ouatani, R. Dedryvère, C. Siret, P. Biensan, S. Reynaud, P. Iratçabal, D. Gonbeau, *J. Electrochem. Soc.* **2009**, *156*, A103.
[23] M. Herstedt, D. P. Abraham, J. B. Kerr, K. Edström, *Electrochim. Acta* **2004**, *49*, 5097.
[24] D. Ensling, M. Stjerndahl, A. Nytén, T. Gustafsson, J. O. Thomas, *J. Mater. Chem.* **2009**, *19*, 82.
[25] B. S. Parimalam, B. L. Lucht, *J. Electrochem. Soc.* **2018**, *165*, A251.
[26] D. Aurbach, B. Markovsky, A. Shechter, Y. Ein-Eli, H. Cohen, *J. Electrochem. Soc.* **1996**, *143*, 3809.
[27] D. Aurbach, I. Weissman, A. Schechter, H. Cohen, *Langmuir* **1996**, *12*, 3991.
[28] D. Aurbach, *J. Power Sources* **2000**, *89*, 206.
[29] M. T. Ong, O. Verners, E. W. Draeger, A. C. T. van Duin, V. Lordi, J. E. Pask, *J. Phys. Chem. B* **2015**, *119*, 1535.
[30] D. M. Seo, S. Reininger, M. Kutcher, K. Redmond, W. B. Euler, B. L. Lucht, *J. Phys. Chem. C* **2015**, *119*, 14038.
[31] X.-B. Cheng, R. Zhang, C.-Z. Zhao, F. Wei, J.-G. Zhang, Q. Zhang, *Adv. Sci.* **2016**, *3*, 1500213.
[32] Y. Wang, T. Matsuyama, M. Deguchi, A. Hayashi, A. Nakao, M. Tatsumisago, *J. Ceram. Soc. Jpn.* **2016**, *124*, 597.
[33] J. Tsuji, M. Fujita, Y. Haruyama, K. Kanda, S. Matsui, N. Ozawa, T. Yao, K. Taniguchi, *Anal. Sci.* **2005**, *21*, 779.
[34] W. Xiong, Q. Hu, S. Liu, *Anal. Methods* **2014**, *6*, 5708.
[35] S. V. Sazhin, K. L. Gering, M. K. Harrup, H. W. Rollins, *J. Electrochem. Soc.* **2014**, *161*, A393.

© 2018 WILEY-VCH Verlag GmbH & Co. KGaA, Weinheim